

Nonequilibrium 2PI evolution of the $O(N)$ model with longitudinal expansion

Yoshitaka Hatta^a and Akihiro Nishiyama^b

^a Faculty of Pure and Applied Sciences, University of Tsukuba, Tsukuba, Ibaraki 305-8571, Japan

^b Maskawa Institute for Science and Culture, Kyoto Sangyo University, Kyoto 603-8555, Japan

Abstract

Motivated by the problem of thermalization in heavy-ion collisions, we present numerical simulations of the nonequilibrium evolution of the $O(N)$ model in $1+2$ dimensions with longitudinal expansion and in the presence of a background field. We work in the NLO approximation of the $1/N$ expansion and consider both the strong and weak coupling cases. Special emphasis is put on the difference between the 2PI formalism and the classical statistical approach. In the 2PI case at strong coupling, we find some evidence of the Bose–Einstein (exponential) distribution in the expanding system.

1. Introduction

Understanding how and when thermalization is achieved in the fireball created in heavy-ion collision experiments is one of the most pressing, but difficult questions in physics of the Quark Gluon Plasma (QGP). The system starts out with a very peculiar initial condition described by the Color Glass Condensate (CGC) framework [1], and eventually ends up with the hydrodynamic regime characterized by the thermodynamic properties of QCD. The transient regime in between is a ‘missing link’ about which our knowledge is severely limited due to the highly nonlinear dynamics of QCD which is furthermore complicated by the one-dimensional expansion of the system.

Analytical insights are available for certain aspects of the evolution, and various scenarios for thermalization have been put forward. [See [2] and references therein.] But if one wants to go beyond parametric estimates and get the whole evolution under quantitative control, numerical simulations based on the first principles seem to be necessary. So far, simulations based on the classical statistical approximation have proven to be very practical for this purpose [3, 4, 5, 6, 7]. These simulations nicely demonstrate, among others, the exponential growth of soft gluons triggered by the decay of classical fields. However, they also indicate that in the weak coupling picture the unstable regime develops in an unrealistically (from the viewpoint of heavy-ion phenomenology) large span of time. Besides, the classical statistical approximation is a low-momentum effective theory, so ‘thermalization’ achieved in this framework is the classical Rayleigh–Jeans type, and not the quantum Bose–Einstein distribution or the Boltzmann (exponential) distribution which is often regarded as a signal of the QGP in heavy-ion

collisions. It is then difficult to tell whether one can form the truly equilibrated QGP on a reasonable time scale, or just some far-from-equilibrium gluonic matter which mimics the QGP by acquiring a constant energy–pressure relation (‘equation of state’) due to the phenomenon of prethermalization [8].

In principle, the latter difficulty can be solved by the two-particle irreducible (2PI) formalism which has a variety of applications in nonequilibrium physics and has been recently discussed in the context of heavy-ion collisions in the CGC picture [9] (see, also, [10]). In the 2PI formalism, the Bose–Einstein distribution is guaranteed as it consistently includes the relevant terms responsible for the quantum equilibration. However, unlike the classical statistical approach, usually the collision terms in the 2PI approach are evaluated to fixed order in the coupling constant. While such an approximation may be justified for certain purposes, in the presence of instability at weak coupling it will break down in the soft sector because higher order loop diagrams, proportional to large powers of the particle density, are no longer suppressed at the height of instability.

Given that the classical statistical approach and the 2PI formalism have their own advantages (and disadvantages), one may hope to find a unified approach which captures both these advantages in a complementary manner. Unfortunately such a formalism is not available in QCD at the moment. There is, however, one (and only one) known example where this can be done—It is the scalar $O(N)$ theory at large N [11]. To next-to-leading order (NLO) in the $1/N$ expansion, one can resum the 2PI loop diagrams (including the terms omitted in the classical statistical approach) to all orders in the coupling constant. It is thus a very attractive toy model from which one can learn important lessons for QCD. Numerical simulations of this model have been previously performed in the flat coordinates [12, 13]. In this paper we report the result of numerical simulations of this model in (1+2)–dimensions with one–dimensional expansion (one time dimension, one transverse dimension, and one longitudinal (expanding) dimension) and in the presence of a background field. Our main focuses are the difference between the 2PI and the classical statistical approaches, and the impact of longitudinal expansion on the equilibration process. For previous 2PI simulations in (spherically) expanding systems, see [14].

2. The model

Our model field theory is the $O(N)$ –symmetric $\lambda\phi^4$ theory in (1+2)–dimensions $x^\mu = (t, x_T, z)$

$$S = \int dt dx_T dz \left(\frac{1}{2} \partial_\mu \phi_a \partial^\mu \phi_a - \frac{1}{2} m^2 \phi_a \phi_a - \frac{\lambda \sigma}{4! N} (\phi_a \phi_a)^2 \right), \quad (1)$$

where $a = 1, 2, \dots, N$. λ is the dimensionless coupling constant and the dimensionful parameter σ sets the energy scale of the problem. We assume that the system is undergoing one–dimensional expansion in the z –direction. It is then convenient to switch to the ‘ τ – η ’ coordinates defined by

$$\tau = \sqrt{t^2 - z^2}, \quad \eta = \tanh^{-1} \frac{z}{t}. \quad (2)$$

τ is the so–called proper time, and η is the rapidity. In these coordinates, the action reads

$$S = \int \tau d\tau dx_T d\eta \left(\frac{1}{2} (\partial_\tau \phi_a)^2 - \frac{1}{2\tau^2} (\partial_\eta \phi_a)^2 - \frac{1}{2} (\partial_T \phi_a)^2 - \frac{1}{2} m^2 \phi_a \phi_a - \frac{\lambda \sigma}{4! N} (\phi_a \phi_a)^2 \right), \quad (3)$$

and the classical equation of motion takes the form

$$\left(\partial_\tau^2 + \frac{1}{\tau} \partial_\tau - \frac{1}{\tau^2} \partial_\eta^2 - \partial_T^2 + m^2 + \frac{\lambda\sigma}{6N} \phi_b \phi_b \right) \phi_a = 0. \quad (4)$$

We shall be interested in the evolution of the system characterized by a nonzero field expectation value at the initial time $\tau = \tau_0 \approx 0$

$$\frac{\langle \phi_a(\tau_0) \rangle}{\sqrt{\sigma}} = \delta_{a1} \sqrt{\frac{6N}{\lambda}}, \quad (5)$$

which we take to be boost invariant (independent of η) and, for simplicity, homogeneous (independent of x_T). Such a background field is to mimic the initial condition of heavy-ion collisions in the color glass condensate picture. In that case, weak (QCD) coupling is assumed so that the classical gluon fields are strong $A^\mu \sim \mathcal{O}(1/\sqrt{\alpha_s}) \gg 1$. Here we relax this assumption and treat λ as a free parameter.

At $\tau > \tau_0$ the classical field decays, and fuels energy for quantum fluctuations to grow. The latter is characterized by the statistical function

$$F_{ab}(x, x') = \frac{1}{2} \langle \{ \phi_a(x), \phi_b(x') \} \rangle - \langle \phi_a(x) \rangle \langle \phi_b(x') \rangle, \quad (6)$$

and the spectral function

$$\rho_{ab}(x, x') = i \langle [\phi_a(x), \phi_b(x')] \rangle. \quad (7)$$

We choose the initial condition such that $\langle \phi_a(\tau) \rangle = 0$ for $a \neq 1$ at all times, and introduce the $O(N-1)$ -symmetric notation $F_{11} \equiv F_{\parallel}$, $F_{22} = F_{33} = \dots = F_{NN} \equiv F_{\perp}$. Since the classical field is independent of x_T and η , we work in the Fourier space and denote the conjugate momenta to x_T and η by p_T and p_η , respectively.

The evolution of the system is described by the following set of coupled equations ('Kadanoff-Baym equation') for $\langle \phi \rangle$, F and ρ :

$$\left[\partial_\tau^2 + \frac{1}{\tau} \partial_\tau + m^2 + \frac{\lambda\sigma}{6N} \left(\phi^2(\tau) + 3F_{11}(\tau, \tau) + \sum_{b \neq 1} F_{bb}(\tau, \tau) \right) \right] \phi(\tau) = - \int_{\tau_0}^{\tau} \tau' d\tau' \Sigma_{11}^\rho(\tau, \tau') \phi(\tau'), \quad (8)$$

where

$$F(\tau, \tau) \equiv \int \frac{dp_T dp_\eta}{(2\pi)^2} F(\tau, \tau, p_T, p_\eta), \quad (9)$$

and $\langle \phi_1(\tau) \rangle$ is simply denoted as $\phi(\tau)$. The equations for the statistical and the spectral functions are

$$\left[\left(\partial_\tau^2 + \frac{1}{\tau} \partial_\tau + \frac{p_\eta^2}{\tau^2} + p_T^2 \right) \delta_{ab} + M_{ab}^2(\phi) \right] F_{bc}(\tau, \tau', p) = - \int_{\tau_0}^{\tau} \tau'' d\tau'' \Sigma_{ab}^\rho(\tau, \tau'', p) F_{bc}(\tau'', \tau', p) + \int_{\tau_0}^{\tau'} \tau'' d\tau'' \Sigma_{ab}^F(\tau, \tau'', p) \rho_{bc}(\tau'', \tau', p), \quad (10)$$

$$\left[\left(\partial_\tau^2 + \frac{1}{\tau} \partial_\tau + \frac{p_\eta^2}{\tau^2} + p_T^2 \right) \delta_{ab} + M_{ab}^2(\phi) \right] \rho_{bc}(\tau, \tau', p) = - \int_{\tau'}^\tau \tau'' d\tau'' \Sigma_{ab}^\rho(\tau, \tau'', p) \rho_{bc}(\tau'', \tau', p), \quad (11)$$

where the effective mass term is

$$M_{ab}^2(\phi) = m^2 \delta_{ab} + \frac{\lambda\sigma}{6N} (F_{cc}(\tau, \tau) + \phi^2) \delta_{ab} + \frac{\lambda\sigma}{3N} (F_{ab}(\tau, \tau) + \phi^2 \delta_{a1} \delta_{b1}). \quad (12)$$

The self energies Σ_{ab}^F and Σ_{ab}^ρ are evaluated in the 2PI formalism to next-to-leading order (NLO) approximation in the $1/N$ expansion. Their expressions are rather lengthy and are not reproduced here. We refer the reader to the original paper [11] and, importantly for the present purpose, its extension [15] to systems with a certain class of curved coordinates including the τ - η coordinates.

3. Numerical simulations: Setup

Thanks to the manifestly causal structure, the equations (8)–(11) can be straightforwardly solved on a lattice. We consider a lattice of size 64×64 in the momentum space with the periodic boundary condition. The momentum and time are discretized as

$$\frac{p_T}{\sigma} = \frac{2\pi n_T}{64a_T\sigma} = \frac{\pi n_T}{64}, \quad p_\eta = \frac{2\pi n_\eta}{64a_\eta} = \frac{\pi n_\eta}{16}, \quad -32 \leq n_T, n_\eta \leq 32, \quad (13)$$

$$\tau = na_t, \quad \tau_0 = 10a_t, \quad (14)$$

where we have chosen the lattice spacings $a_T = 2/\sigma$, $a_\eta = 0.5$, and $a_t = 0.4/\sigma$. Due to the symmetry of the problem $p \leftrightarrow -p$, the actual simulations may be performed on a 32×32 lattice by restricting to the region $p_\eta, p_T > 0$. As for the mass parameter, we take $m = 0.1\sigma$.¹

The initial conditions are determined as follows. In the noninteracting theory, and in the expanding coordinates, the statistical function takes the generic form (see Appendix)

$$F_0(\tau, \tau', p) = \frac{\pi}{2} \text{Re} \left\{ H_{ip_\eta}^{(2)}(m_T \tau) H_{ip_\eta}^{(1)}(m_T \tau') \right\} \left(\frac{1}{2} + n_p \right), \quad (15)$$

where² $m_T = \sqrt{p_T^2 + m^2}$ and

$$n_p \delta^{(2)}(p - q) = \langle a_p^\dagger a_q \rangle, \quad (17)$$

¹The bare mass m is negligible almost everywhere when solving the evolution equation. The only reason we keep m finite is to avoid an IR divergence in the integral (21) in our renormalization prescription, $\int dp_T F_0 \sim \sum_{n_T} F_0$ at $n_T = 0$.

²In actual simulations, the transverse momenta squared is replaced by

$$\frac{p_T^2}{\sigma^2} \rightarrow \frac{2}{(a_T\sigma)^2} \left(1 - \cos \frac{\pi n_T}{32} \right) = \frac{1}{2} \left(1 - \cos \frac{\pi n_T}{32} \right), \quad (16)$$

in order to reduce lattice artifacts.

is an arbitrary distribution of pre-existing quanta. We assume that the initial state contains only the classical field (5) and no on-shell particle excitations. This means $n_p(\tau_0) = 0$, and the classical field induces an effective mass term for the fluctuation. Our initial conditions are thus given by

$$\begin{aligned} F_{\parallel}(\tau, \tau', p) &= \frac{\pi}{4} \text{Re} \left\{ H_{ip_{\eta}}^{(2)}(m_{\parallel}\tau) H_{ip_{\eta}}^{(1)}(m_{\parallel}\tau') \right\}, & m_{\parallel} &= \sqrt{p_T^2 + m^2 + 3\sigma^2}, \\ F_{\perp}(\tau, \tau', p) &= \frac{\pi}{4} \text{Re} \left\{ H_{ip_{\eta}}^{(2)}(m_{\perp}\tau) H_{ip_{\eta}}^{(1)}(m_{\perp}\tau') \right\}, & m_{\perp} &= \sqrt{p_T^2 + m^2 + \sigma^2}, \end{aligned} \quad (18)$$

evaluated at $\tau = \tau' = \tau_0$.

Since the equations (8)–(11) are second order in the τ -derivative, we must also specify the first derivatives. For the classical field, we take

$$\partial_{\tau}\phi(\tau) \Big|_{\tau_0} = 0, \quad (\tau_0 \rightarrow 0), \quad (19)$$

again motivated by the situation in the CGC case [1], whereas $\partial_{\tau}F(\tau, \tau_0)|_{\tau_0}$ and $\partial_{\tau}\partial_{\tau'}F(\tau, \tau')|_{\tau_0}$ are computed from (18). The initial condition for the spectral function is fixed by the canonical commutation relation

$$\rho_{ab}(\tau_0, \tau_0, p) = 0, \quad \partial_{\tau}\rho_{ab}(\tau, \tau_0) \Big|_{\tau=\tau_0} = \delta_{ab} \frac{1}{\tau_0}. \quad (20)$$

(20) is actually satisfied for all values of τ even in the interacting theory, so it can be used as a check of the simulation.

Concerning renormalization, in (1+2)-dimensions the tadpole self-energy (9) is linearly divergent. We renormalize this by subtracting the free part at each step of the evolution

$$F(\tau, \tau) \rightarrow \int \frac{d^2p}{(2\pi)^2} (F(\tau, \tau, p) - F_0(\tau, \tau, p)), \quad (21)$$

where $\int F_0$ is computed from (15) (with $n_p = 0$). There is also a logarithmic divergence in the ‘sunset’ diagram which appears in Σ at two loops. Though in principle this requires an extra term in the mass renormalization (see, e.g., [16]), in this work we do not perform the renormalization of logarithmic divergences.

As stated in the introduction, our main interest is the difference between the full 2PI calculation and its classical statistical approximation. We thus show the result of the latter simulation as well. In the present context (at NLO in $1/N$), this simply amounts to neglecting, in the set of equations (8)–(11), terms quadratic in ρ ’s when they appear in conjunction with terms quadratic in F ’s [12]. Note that we still perform the renormalization (21), so in this sense our ‘classical’ simulation is not exactly the same as the other classical statistical simulations where cut-off dependent tadpoles are kept as they are.

Furthermore, in order to see the effect of the expansion, we also perform simulations in the non-expanding case in the flat coordinates (t, x_T, z) on an isotropic lattice $a_z = 2/\sigma = a_T$, $a_t = a_{\tau}$. The parameters are chosen such that the relation $a_z = \tau_0 a_{\eta}$ (from $dz = \tau d\eta$ at midrapidity $\eta = z = 0$) is satisfied at the initial time $t_0 = \tau_0$. The initial conditions for the classical field are the same as in the expanding case (up to the replacement $\tau \rightarrow t$), while those

for the F , ρ -functions are

$$\begin{aligned} F_{\parallel}(t_0, t_0, p) &= \frac{1}{2\sqrt{p^2 + m^2 + 3\sigma^2}}, & (p^2 = p_T^2 + p_z^2), \\ F_{\perp}(t_0, t_0, p) &= \frac{1}{2\sqrt{p^2 + m^2 + \sigma^2}}, \end{aligned} \quad (22)$$

$$\rho_{ab}(t, t, p) = 0, \quad \partial_t \rho_{ab}(t, t', p) \Big|_{t=t'} = \delta_{ab}, \quad (23)$$

and $\partial_t F(t, t_0, p)|_{t=t_0} = 0$, etc. (c.f., (A.12)).

The degree of thermalization may be inferred from the functional form of F at large time. In the non-expanding case, we extract the effective distribution $n_p(t)$ from the data using the prescription

$$\frac{1}{\omega_p} + n_p(t) \equiv \sqrt{F(t, t', p) \partial_t \partial_{t'} F(t, t', p)} \Big|_{t=t'}, \quad (24)$$

which is often employed in the literature (e.g., Refs. [12, 14]). The ‘equilibrium’ distribution in the expanding case is not known, nor is it clear if such a distribution is theoretically well-defined in our anisotropically expanding system. We try, however, the following ansatz for the late-time behavior of the correlation function (cf. Eqs. (15) and (A.10))

$$F(\tau, \tau, p) = \frac{C}{\omega_p \tau} \left(\frac{1}{2} + \frac{1}{e^{\omega_p/T} - 1} \right), \quad \omega_p = \sqrt{p_T^2 + m_{eff}^2}, \quad (25)$$

and see if we can identify an exponentially decaying (in p_T) component by adjusting the parameter $C(\tau) \approx 1$ (‘field strength renormalization’). At the same time we determine the fitting parameters $T(\tau)$ (‘temperature’) and $m_{eff}(\tau)$ (‘thermal effective mass’).

Note that, as already implied by (25), we neglect the dependence of F on p_{η} , or equivalently, the longitudinal momentum $p_z \sim p_{\eta}/\tau$ at late times. Indeed, in our simulations F becomes independent of p_{η} after some time because p_{η} enters the equation of motion in the form $(p_{\eta}/\tau)^2$ (see, also, (A.13)). In order to see the dependence on $p_z \sim p_{\eta}/\tau$, we have to use a considerably larger p_{η} cutoff such that the typical value of p_{η}/τ at large τ is of the same order as the p_T cutoff. We do not perform such simulations in this paper both from technical and phenomenological reasons. Technically, 2PI simulations in a very large (and anisotropic) lattice is computationally very expensive. Besides, the product of Hankel functions used in the initial condition (18) behaves badly when p_{η} becomes larger than around 10. [Our current cutoff is $p_{\eta} < 2\pi$.] Phenomenologically, in heavy-ion collisions, experimentalists usually measure the p_T dependence, but not the p_z dependence (to our knowledge) because the latter is not boost invariant and depends sensitively on the collision energy. Our primary goal here is to reproduce the exponential p_T dependence around midrapidity $\eta \approx 0$ which is well established experimentally, and for this purpose the inclusion of finite- p_z modes is presumably not very crucial: Due to the redshift $p_z \sim p_{\eta}/\tau$, the relevant values of p_z naturally decrease with time, and modes with finite p_z escape from the midrapidity region and do not affect much the p_T distribution there.

4. Numerical simulations: Results

In this section we present the numerical solution of the equations (8)–(11) obtained after 1600 steps ($\tau/\tau_0 = 160$) of evolution in time. We run $2^3 = 8$ different simulations corresponding to the following cases: (i) weak $\lambda = 10^{-4}$ and strong $\lambda = 10$ coupling, (ii) 2PI and the classical statistical approximation, (iii) with and without longitudinal expansion. All the results below are for $N = 4$.

4.1. Weak coupling

Let us first present the results at weak coupling $\lambda = 10^{-4}$. Fig. 1 shows the time evolution of the classical field (in units of $\sqrt{\sigma}$) in the expanding case (left) and non-expanding case (right). In the expanding case, the amplitude of ϕ decays very fast and has a characteristic shape. This can be understood analytically [17] at weak coupling where the evolution of ϕ is largely determined by the classical equation. A detailed analysis gives $\phi(\tau) \sim 1/\tau^{1/3}$, while the period of oscillation is constant in $\tau^{2/3}$, meaning that the effective period becomes longer at larger τ . These tendencies are clearly visible. In the non-expanding case, on the other hand, the amplitude is constant in time at the classical level, and diminishes only as a result of its coupling to quantum fluctuations. The difference between the full 2PI and the classical statistical approximation is unnoticeable, hence we did not plot the latter.

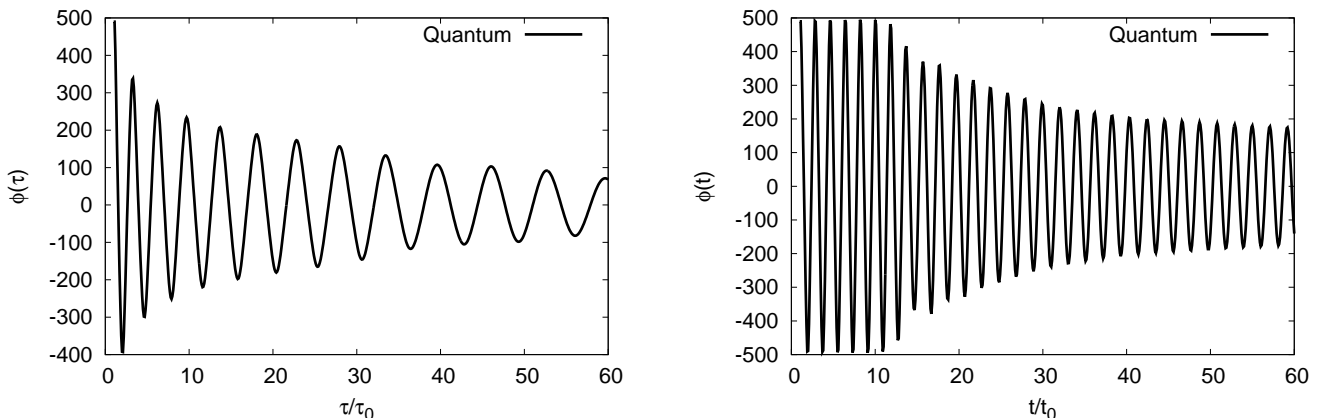


Figure 1: Time evolution of the classical field at weak coupling $\lambda = 10^{-4}$. Left: with expansion; Right: without expansion.

Next, in Fig.2 we plot $F_{\parallel}(\tau, \tau, p_T, p_{\eta} = 0)$ (expanding case, left) and $F_{\parallel}(t, t, p_T, p_z = 0)$ (non-expanding case, right)³ for three different values of $p_T/\sigma = \frac{\pi}{64}n_T$, $n_T = 0, 8, 16$. We confirm the parametric resonance previously observed at weak coupling [17]. We also see that the effect of the expansion is huge, suppressing the magnitude of F by several orders of magnitude compared with the non-expanding case. Actually, the suppression is so strong that the equal-time correlator $F(\tau, \tau, p)$, which should be a positive quantity, turns slightly negative in some momentum modes beyond $\tau \gtrsim 50\tau_0$. We presume this is because of large errors incurred when very large and very small numbers (which differ by $\sim 10^6$) coexist, or

³In the nonexpanding case, we actually plot $\sigma F(t, t, p)$ to make it dimensionless.

simply due to an artifact of the smallness of our lattice.⁴ We note, however, that $F(\tau, \tau, p)$ turns positive again for all momentum modes at later times $\tau \gtrsim 100\tau_0$, and shows a smooth, nonthermal distribution in p_T .

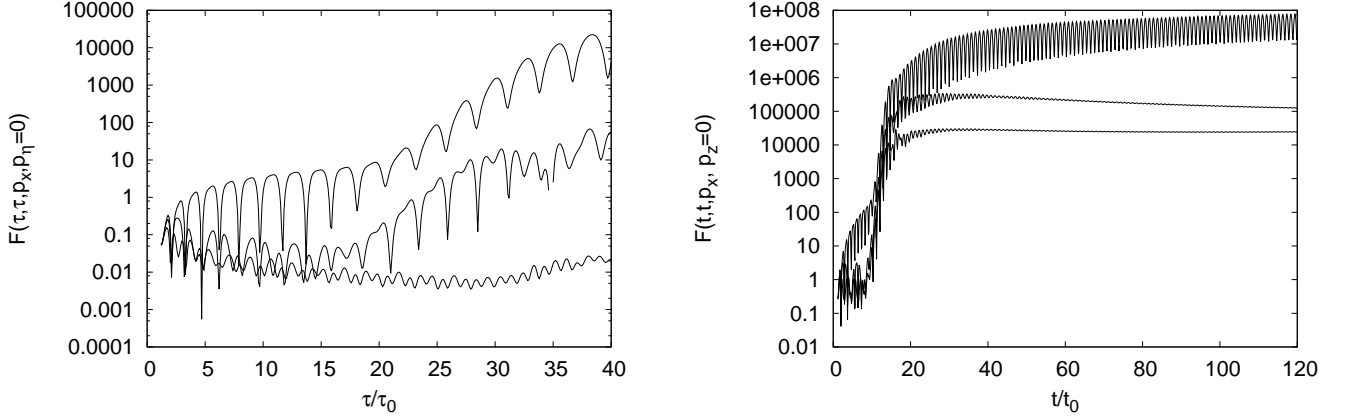


Figure 2: Time evolution of the statistical function at weak coupling $\lambda = 10^{-4}$ for three different values of n_T : $n_T = 0, 8, 16$ (from top to bottom). Left: with expansion. Right: without expansion.

Again, there is no discernible difference between the 2PI and the classical statistical approximation. This is understandable in the non-expanding case as F becomes very large and the condition $FF \gg \rho\rho$ is always satisfied. [Remember that ρ is an $\mathcal{O}(1)$ quantity due to the constraint (23).] In the expanding case, it is simply because the whole collision term is small and contributes very little to the evolution. In either case, the lack of any difference in the two simulations indicates that the system is far from the true equilibrium state even at the final time $\tau/\tau_0 = 160$. The p_T -distribution is so overpopulated in the soft region that it is entirely impossible to find any hint of ‘subtle’ quantum effects like the exponential distribution. Presumably we have to wait for a much longer time to see the difference, but this is beyond the scope of the present work.

4.2. Strong coupling

We now turn to the results at strong coupling $\lambda = 10$. In Fig. 3 we plot the time evolution of the classical field. Compared to the weak coupling case (Fig. 1), the decay of the amplitude is faster because the transfer of energy to quantum fluctuations is more efficient at strong coupling. Still, the difference between the 2PI and classical simulations is barely noticeable.

Next we plot the statistical function at strong coupling in Fig. 4 which should be compared with the weak coupling counterpart Fig. 2. Because the magnitude of the classical field is smaller, the parametric resonance is less pronounced, and is basically unrecognizable in the expanding case. At least in the present model, this ineffectiveness of the instability appears to be the key to achieve an early thermalization. Indeed, we get a reasonable fit of the momentum distribution using the ansatz (25). Fig. 5 shows the distribution $n_p(\tau) \equiv \tau\omega_p F(\tau, \tau, p)/C - \frac{1}{2}$

⁴This problem does not seem to occur in the Monte Carlo simulation (rather than solving differential equations) of the classical statistical theory on a larger lattice [17]. It is computationally very expensive and not realistic for us to increase the lattice size.

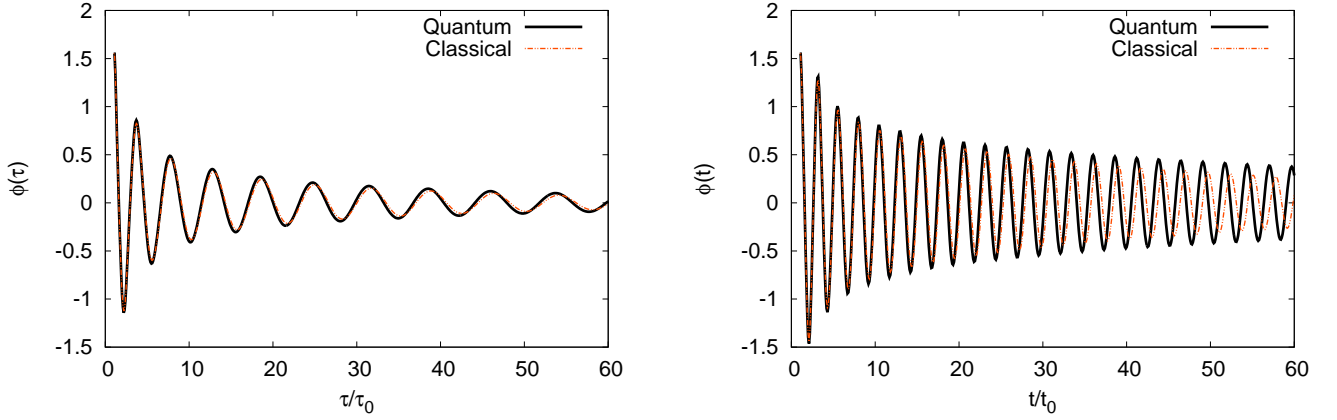


Figure 3: Time evolution of the classical field at strong coupling $\lambda = 10$. Left: with expansion; Right: without expansion. Both the 2PI result (black solid line) and the classical statistical result (red dashed line) are shown, although the difference is very small.

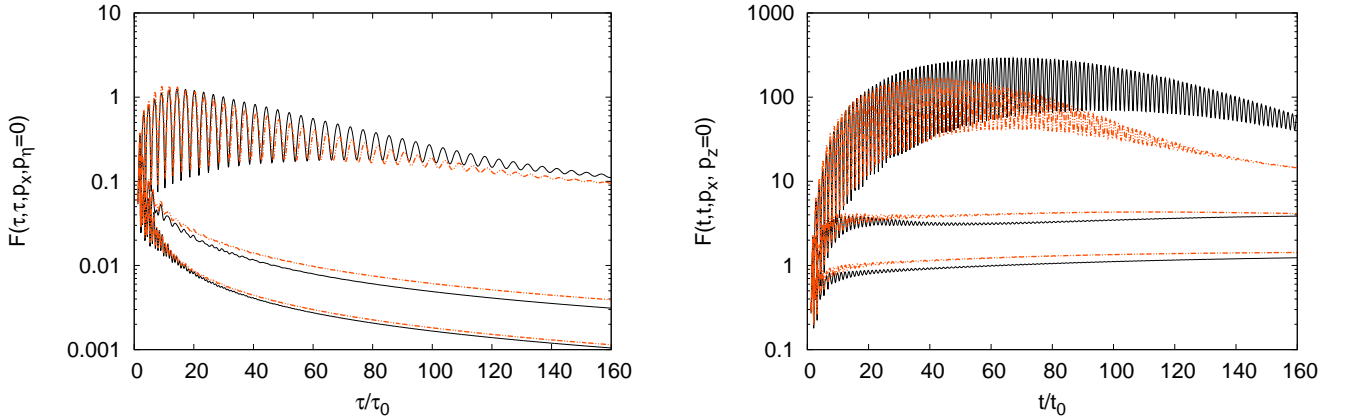


Figure 4: Time evolution of the statistical function at strong coupling $\lambda = 10$ for three different values of n_T : $n_T = 0$, $n_T = 8$, $n_T = 16$ (from top to bottom). Left: with expansion. Right: without expansion.

in the expanding case at two values of τ : $\tau/\tau_0 = 50$ and $\tau/\tau_0 = 150$. The fitting parameters are found to be

	C	T/σ	m_{eff}/σ
$\tau/\tau_0 = 50$	0.905	0.354	0.0817
$\tau/\tau_0 = 150$	0.913	0.413	0.0586

where $C \approx 1$, as expected. The exponential behavior actually starts to show up already around $\tau/\tau_0 \gtrsim 40$. The difference between the 2PI and the classical statistical approximation is now manifest. In the latter case (red lines), the distribution plunges and becomes negative in the high- p_T region⁵ (around $n_T = 15 \sim 20$) where the quantum (2PI) distribution still keeps up with the exponential trend.

⁵This is an expected behavior because the equilibrium distribution in the classical statistical theory corresponds

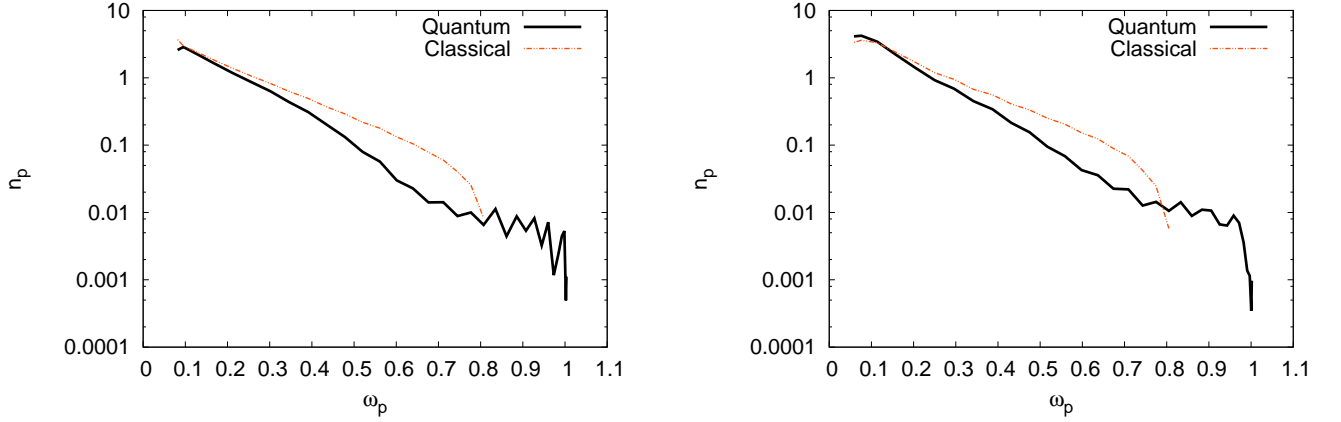


Figure 5: The distribution n_p as a function of ω_p at strong coupling $\lambda = 10$ in the expanding case. Left: $\tau = 50\tau_0$. Right: $\tau = 150\tau_0$. The distribution from the classical statistical approximation (red line) turns negative beyond $\omega_p \gtrsim 0.8$.

Similarly, in the non-expanding case we plot in Fig. 6 the distribution n_p defined in (24) as a function of $p = \sqrt{p_T^2 + p_z^2}$. Again the distribution in the 2PI case develops an exponential tail already at $t = 50t_0$, but the classical distribution follows a power law and becomes negative.

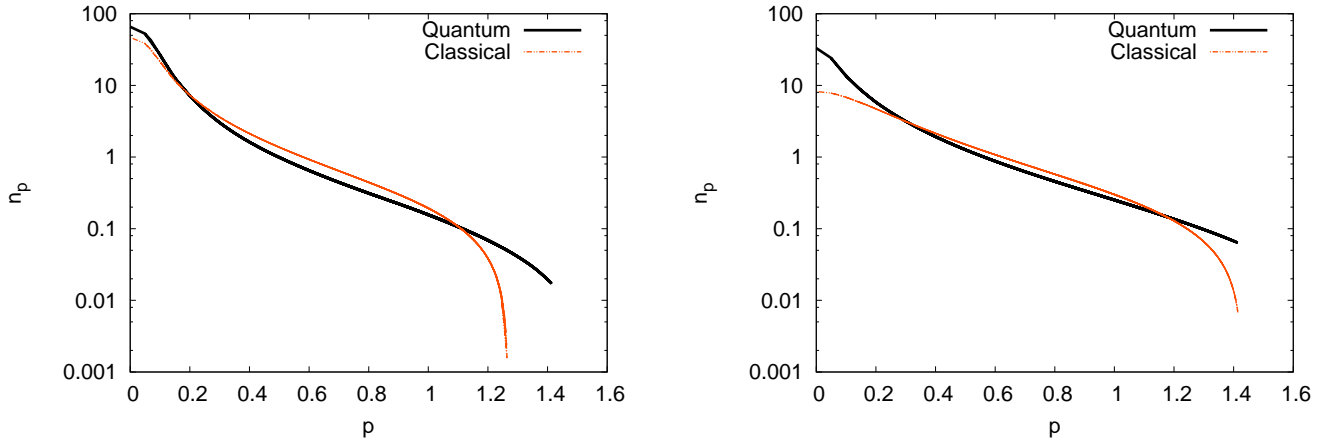


Figure 6: The distribution n_p defined in (24) at strong coupling $\lambda = 10$ without expansion. Left: $t = 50t_0$; Right: $t = 150t_0$.

to the following approximation to the Bose–Einstein distribution

$$\frac{1}{e^{\omega_p/T} - 1} \rightarrow \frac{T}{\omega_p} - \frac{1}{2}. \quad (26)$$

5. Conclusions

In this paper, we have for the first time performed the 2PI simulation of the $O(N)$ model with longitudinal expansion. This model is unique in that, to NLO in the $1/N$ expansion, one can resum the 2PI diagrams to all orders in the coupling constant. Therefore, it is valid for all values of the coupling and also in the presence of violent instabilities. At weak coupling, the parametric resonance is strong and the classical statistical approach is an extremely good approximation. This means, however, that we cannot see any hint of the quantum equilibration within the time range explored in this work. Just for a (naive) comparison, we note that in heavy-ion collisions one would choose $\tau_0 \sim 1/Q_s \sim 0.1$ fm (the inverse of the saturation momentum) and the lifetime of the QGP is $\lesssim 5$ fm, so in practice we have a constraint $\tau/\tau_0 \lesssim 50$. Thus, in order to achieve the truly equilibrated system (not just the establishment of an equation of state) in such a short time, pictures based on the weak coupling limit may not be a good starting point. Instead, we have seen that in the 2PI simulation at strong coupling the difference from the classical statistical approximation does show up within a reasonable time scale, and plays a crucial role in developing the Bose–Einstein (or the exponential) distribution in p_T .

Acknowledgments

We thank Yukawa Institute for Theoretical Physics for providing computational facilities essential for the completion of this work.

Appendix A. Free correlation function

The quantization of the scalar field in the τ – η coordinates was studied in [18]. In (1+2)–dimensions, the canonical commutation relation

$$[\phi(\tau, x_T, \eta), \tau \partial_\tau \phi(\tau, x'_T, \eta')] = i\delta(\eta - \eta')\delta(x_T - x'_T), \quad (\text{A.1})$$

admits the following mode expansion

$$\phi(x) = \int dp_T dp_\eta \left[a_{p_T, p_\eta} \xi_{p_T, p_\eta}(x) + a_{p_T, p_\eta}^\dagger \xi_{p_T, p_\eta}^*(x) \right], \quad (\text{A.2})$$

Here the one–particle wavefunction

$$\begin{aligned} \xi_{p_T, p_\eta}(x) &= \frac{e^{-\pi p_\eta/2}}{4\pi^{1/2}} H_{-ip_\eta}^{(2)}(m_T \tau) e^{-ip_\eta \eta - ip_T x_T}, \\ \int \tau dx_T d\eta \xi_{p'_T, p'_\eta}^*(x) i \overleftrightarrow{\frac{\partial}{\partial \tau}} \xi_{p_T, p_T}(x) &= \delta(p_\eta - p'_\eta) \delta(p_T - p'_T), \end{aligned} \quad (\text{A.3})$$

with $m_T = \sqrt{p_T^2 + m^2}$, is normalized such that the commutation relation of a and a^\dagger takes the form

$$[a_{p_T, p_\eta}, a_{p'_T, p'_\eta}^\dagger] = \delta(p_T - p'_T) \delta(p_\eta - p'_\eta). \quad (\text{A.4})$$

The statistical and the spectral functions of the free theory are easily calculated

$$F(\tau, \tau', p) = \frac{1}{2} \langle 0 | \{ \phi(\tau, p), \phi(\tau', -p) \} | 0 \rangle = \frac{\pi}{4} \text{Re} \left(H_{ip_\eta}^{(2)}(m_T \tau) H_{ip_\eta}^{(1)}(m_T \tau') \right), \quad (\text{A.5})$$

$$\rho(\tau, \tau', p) = i \langle 0 | [\phi(\tau, p), \phi(\tau', -p)] | 0 \rangle = -\frac{\pi}{2} \text{Im} \left(H_{ip_\eta}^{(2)}(m_T \tau) H_{ip_\eta}^{(1)}(m_T \tau') \right). \quad (\text{A.6})$$

The approximate form at early times $\tau, \tau' \rightarrow 0$ is

$$F(\tau, \tau, p) \approx \frac{1}{2p_\eta \tanh p_\eta \pi} + \frac{\cos \left(2p_\eta \ln \frac{m_T \tau}{2} - 2\theta(p_\eta) \right)}{2p_\eta \sinh p_\eta \pi}, \quad (\text{A.7})$$

$$\rho(\tau, \tau', p) \approx -\frac{1}{p_\eta} \sin \left(p_\eta \ln \frac{\tau'}{\tau} \right), \quad (\text{A.8})$$

where

$$\theta(p_\eta) = \arg \left(\Gamma(ip_\eta) \right), \quad (\text{A.9})$$

is the phase of the gamma function. The late-time behavior $\tau, \tau' \rightarrow \infty$ is

$$F(\tau, \tau', p) \approx \frac{1}{2m_T \sqrt{\tau \tau'}} \cos m_T (\tau - \tau'), \quad (\text{A.10})$$

$$\rho(\tau, \tau', p) \approx \frac{1}{m_T \sqrt{\tau \tau'}} \sin m_T (\tau - \tau'). \quad (\text{A.11})$$

These are similar in form to the corresponding functions in the flat coordinates

$$F(t, t', p) = \frac{1}{2\omega_p} \cos \omega_p (t - t'), \quad \rho(t, t', p) = \frac{1}{\omega_p} \sin \omega_p (t - t'), \quad (\text{A.12})$$

where $\omega_p = \sqrt{p^2 + m^2}$. Finally we note the first subleading term at $\tau = \tau' (\rightarrow \infty)$

$$F(\tau, \tau, p) \approx \frac{1}{m_T \tau} \left(\frac{1}{2} - \frac{p_\eta^2 + \frac{1}{4}}{4m_T^2 \tau^2} \right). \quad (\text{A.13})$$

References

- [1] A. Kovner, L. D. McLerran and H. Weigert, Phys. Rev. D **52**, 3809 (1995) [hep-ph/9505320].
- [2] A. Kurkela and G. D. Moore, JHEP **1112**, 044 (2011) [arXiv:1107.5050 [hep-ph]].
- [3] P. Romatschke and R. Venugopalan, Phys. Rev. Lett. **96**, 062302 (2006) [hep-ph/0510121].
- [4] J. Berges, S. Scheffler and D. Sexty, Phys. Rev. D **77**, 034504 (2008) [arXiv:0712.3514 [hep-ph]].

- [5] T. Kunihiro, B. Muller, A. Ohnishi, A. Schafer, T. T. Takahashi and A. Yamamoto, Phys. Rev. D **82**, 114015 (2010) [arXiv:1008.1156 [hep-ph]].
- [6] K. Dusling, F. Gelis and R. Venugopalan, Nucl. Phys. A **872**, 161 (2011) [arXiv:1106.3927 [nucl-th]].
- [7] J. Berges, S. Schlichting and D. Sexty, arXiv:1203.4646 [hep-ph].
- [8] J. Berges, S. Borsanyi and C. Wetterich, Phys. Rev. Lett. **93**, 142002 (2004) [hep-ph/0403234].
- [9] Y. Hatta and A. Nishiyama, Nucl. Phys. A **873**, 47 (2012) [arXiv:1108.0818 [hep-ph]].
- [10] A. Nishiyama and A. Ohnishi, Prog. Theor. Phys. **125**, 775 (2011) [arXiv:1011.4750 [nucl-th]].
- [11] G. Aarts, D. Ahrensmeier, R. Baier, J. Berges and J. Serreau, Phys. Rev. D **66**, 045008 (2002) [hep-ph/0201308].
- [12] G. Aarts and J. Berges, Phys. Rev. Lett. **88**, 041603 (2002) [hep-ph/0107129].
- [13] A. Arrizabalaga, J. Smit and A. Tranberg, JHEP **0410**, 017 (2004) [hep-ph/0409177].
- [14] A. Tranberg, JHEP **0811**, 037 (2008) [arXiv:0806.3158 [hep-ph]].
- [15] J. Berges and S. Roth, Nucl. Phys. B **847**, 197 (2011) [arXiv:1012.1212 [hep-ph]].
- [16] S. Juchem, W. Cassing and C. Greiner, Phys. Rev. D **69**, 025006 (2004) [hep-ph/0307353].
- [17] J. Berges, K. Boguslavski and S. Schlichting, arXiv:1201.3582 [hep-ph].
- [18] A. Makhlin, hep-ph/9608259.